J Comp Physiol A (2008) 194:795–810
DOI 10.1007/s00359-008-0350-2

ORIGINAL PAPER

Mechanical filtering by the boundary layer and fluid–structure interaction in the superficial neuromast of the fish lateral line system

Matthew J. McHenry · James A. Strother · Sietse M. van Netten

Received: 21 December 2007 / Revised: 10 June 2008 / Accepted: 11 June 2008 / Published online: 16 August 2008

Abstract A great diversity of aquatic animals detects water flow with ciliated mechanoreceptors on the body's surface. In order to understand how these receptors mechanically filter signals, we developed a theoretical model of the superficial neuromast in the fish lateral line system. The cupula of the neuromast was modeled as a cylindrical beam that deflects in response to an oscillating flow field. Its accuracy was verified by comparison with prior measurements of cupular deflection in larval zebrafish (*Danio rerio*). The model predicts that the boundary layer of flow over the body attenuates low-frequency stimuli. The fluid–structure interaction between this flow and the cupula attenuates high-frequency stimuli. The number and height of hair cell kinocilia and the dimensions of the cupular matrix determine the range of intermediate frequencies to which a neuromast is sensitive. By articulating the individual mechanical contributions of the boundary layer and the components of cupular morphology, this model provides the theoretical framework for understanding how a hydrodynamic receptor filters flow signals.

Keywords Fish · Mechanosensation · Hair cells · Biomechanics · Zebrafish

M. J. McHenry (✉) · J. A. Strother
Department of Ecology and Evolution,
University of California, 5205 McGaugh Hall,
Irvine, CA 92697, USA
e-mail: mmchenry@uci.edu

S. M. van Netten
Department of Neurobiophysics, University of Groningen,
Nijenborgh 4, 9747 AG Groningen, The Netherlands

List of symbols

a	radius of cupula at base
a_s	radius of a sphere
b_m	force coefficient for cupular material
b_w	force coefficient for fluid
c	speed of sound in water
C	integration constant
E_m	Young's modulus of cupular matrix
F	stimulus frequency
F_b	buoyant force
F_e	elastic force
F_m	inertial force
F_a	acceleration reaction
F_u	viscous drag
h_h	height of hair bundle
h_c	height of cupula
h_k	height of kinocilia
I	second moment of area
k	viscous drag coefficient
L	hydrodynamic force coefficient
M	bending moment
N	number of hair cells
p	distance between center of sphere and flat plate
q_l	linear spring bundle stiffness
q_t	torsion spring bundle stiffness
r	distance from center of sphere
Re	Reynolds number
S_h	sensitivity of cupula to local flow
S_b	sensitivity of local flow to freestream flow
S_f	sensitivity of cupula to freestream flow
S_l	Sensitivity of local flow to an oscillating sphere
S_s	sensitivity of cupula to oscillating sphere
St	Strouhal number
t	time
U	flow velocity

U_∞	freestream velocity
U_s	flow velocity generated by an oscillating sphere
$U_{s,lin}$	linearized flow velocity generated by vibrating sphere
W	sphere velocity
$\hat{\boldsymbol{x}}$	unit vector along body
z	position along height
$\hat{\boldsymbol{z}}$	unit vector along height
β	boundary layer flow velocity gradient
δ	boundary layer thickness
μ	dynamic viscosity of water
v	cupula deflection
v_s	cupula deflection by vibrating sphere
ρ_m	density of cupular material
ρ_w	density of fluid
ω	angular rate of oscillation

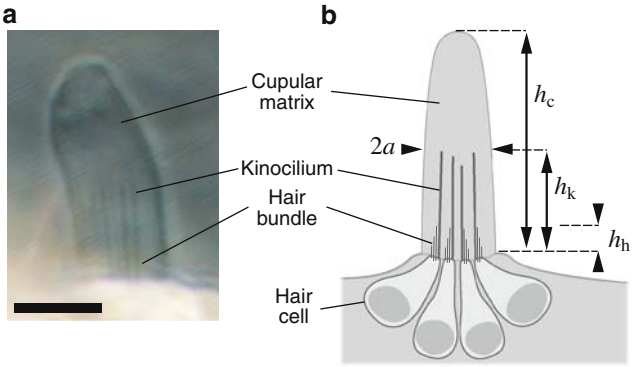

Fig. 1 The morphology of a superficial neuromast. **a** Photograph of the cupula of a superficial neuromast of a zebrafish larva coated with polystyrene microspheres and viewed with Nomarski optics (*scale bar* 10 μm). **b** The morphological parameters of a cupula that factor into the model: the heights of the cupula (h_c), kinocilia (h_k), and stereocilia (h_h), and the radius of the cupula (a)

Introduction

A wide diversity of animals senses water flow with ciliated receptor organs on the surface of their bodies. These hydrodynamic receptors are present in a variety of shapes and sizes among animals as disparate as cnidarians (Arkett and Mackie 1988), tunicates (Bone and Ryan 1978), echinoderms (Moore and Cobb 1986), cephalopods (Budelmann and Bleckmann 1988), fishes (Hofer 1908), and amphibians (Scharrer 1932) (reviewed by Budelmann 1989). Despite the broad phylogenetic distribution of this sensory system, the mechanics that govern hydrodynamic reception are not well understood. It is therefore unclear how sensitivity depends on the morphology of flow receptors or how hydrodynamic interaction with the body affects the signals that they detect. In the interest of resolving these dynamics, the present study develops, verifies, and analyzes a mathematical model of the mechanics of the superficial neuromast of the lateral line system of fishes.

Lateral line receptors may be classified as superficial or canal neuromasts. Superficial neuromasts are located on the surface of the body, where they are thought to sense flow velocity. In contrast, canal neuromasts reside in channels beneath the scales, where they are believed to detect pressure gradients (reviewed by Bleckmann 1994; Coombs and Montgomery 1999; Coombs and van Netten 2006; Janssen 2004; Mogdans et al. 2004; van Netten 2006). Both types of neuromast include a group of hair cells embedded within the epithelium. Kinocilia from these cells extend into a gelatinous matrix that forms the cupula of the neuromast (Fig. 1). When the cupula is subjected to flow, deflections of the kinocilia are transduced into graded potentials across the hair cell membrane by their linkage to a stair-step bundle of mechano-sensitive stereocilia (Harris et al. 1970; Hudspeth and Corey 1977; Hudspeth and Jacobs 1979). The motion of the hair bundles (kinocilia and stereocilia) generates transducer potentials that are encoded by changes in the frequency of action potentials in afferent neurons (Flock 1965). These signals provide the central nervous system with information about water flow around the body.

The flow detected by the lateral line system is filtered by the hydrodynamics of a fish's body. The viscosity of water causes flow close to the body's surface to move slower than the stimulus. This spatial gradient in flow, known as the "boundary layer," has been studied extensively (Lamb 1945; Schlichting 1979). Models of the boundary layer demonstrate that flows close to a surface increase in velocity at greater frequency of oscillation. Therefore, the boundary layer over the surface of a fish's body behaves as a high-pass filter that attenuates low-frequency stimuli (Kuiper 1967; Hassan 1985; Kalmijn 1988; Teyke 1988; Dinklo 2005). The present study considers whether this filter has a substantive influence on flow sensing by superficial neuromasts.

Signal detection by a superficial neuromast depends on mechanical properties of the cupula. The shape and size of the cupula affect both the fluid forces that may be generated by a stimulus and the structural resistance to these forces. A major component of this resistance, the flexural stiffness of the cupula, depends on how many rigid kinocilia are embedded within the compliant cupular matrix (McHenry and van Netten 2007). The deflections of this structure in flow are determined by interdependent structural dynamics and hydrodynamics of the cupula. The filter created by this fluid–structure interaction can only be understood with a theoretical approach that considers both components. Therefore, in addition to examining the role of the boundary layer, we have modeled the fluid–structure

interaction of the cupula in our consideration of mechanical filtering by the superficial neuromast.

Materials and methods

We have developed a model that relates the morphology of a superficial neuromast to its sensitivity over a range of stimulus frequencies. This model considers the boundary layer over the body's surface generated by an oscillating stimulus. It calculates the forces generated by this flow upon and within a cupula by treating this structure as a cylindrical beam (Fig. 2). These forces are described by a fourth-order differential equation, which is referred to as the governing equation. Solutions to the governing equation provide predictions of cupular deflection as a function of its height above the skin. These predictions permit the calculation of the frequency response of a superficial neuromast.

Structural dynamics

The cupula was modeled as two joined beams of different flexural stiffness because the proximal and distal portions of a cupula differ in their material properties (McHenry and van Netten 2007). The flexural stiffness of a beam is equal to the product of its second moment of area, I, and the complex modulus, E, of its material. The complex modulus characterizes the viscoelastic properties of the material and therefore consists of elastic, E' (i.e. Young's modulus), and viscous, E'', components ($E = E' + iE''$, Wainwright et al. 1976). Assuming a cylindrical shape, the second moment of area may be calculated with the following equation (Gere 2001):

$$I = \frac{\pi}{4}a^4, \tag{1}$$

where a is the radius. The distal tip of the cupula is composed entirely of extracellular matrix (McHenry and van Netten 2007). Therefore, the flexural stiffness of the distal beam was calculated as follows (Gere 2001):

$$(EI)_2 = E_\mathrm{m} I_2, \tag{2}$$

where $(EI)_2$ and I_2 are, respectively, the flexural stiffness and second moment of area for the distal cupula, and E_m is the complex modulus of the cupular matrix. In quasi-static mechanical testing, it was found that flexural stiffness of the proximal region varies as a linear function of the number of kinocilia (McHenry and van Netten 2007). Therefore, we calculated the flexural stiffness of this region with the following relationship:

$$(EI)_1 = E_\mathrm{m} I_1 + N(EI)_\mathrm{k}, \tag{3}$$

where $(EI)_1$ is the flexural stiffness of the proximal region, $(EI)_\mathrm{k}$ is the flexural stiffness for an individual kinocilium, n is the number of kinocilia (equal to the number of hair cells), and I_1 is the second moment of area for the proximal cupula.

The structural forces generated by a beam depend on its flexural stiffness and mass. If the beam's deflections are sufficiently small that its arclength approximates its height, the Euler–Bernoulli equations predict the following relationship for the elastic force acting upon a beam element of height dz (Gere 2001):

$$F_\mathrm{e}(z) = EIv''''(z)\mathrm{d}z. \tag{4}$$

where F_e is the elastic force, and $v''''(z)$ is the fourth derivative of deflection with respect to beam height, z (Gere 2001). The mass of a beam plays an increasingly prominent role in the dynamics at high oscillation frequencies. We calculated the inertial force as the product of the mass ($\rho\pi a^2\mathrm{d}z$) and acceleration ($-v(z)\omega^2$) of a beam element:

$$F_\mathrm{m}(z) = -\pi\rho_\mathrm{m}a^2\omega^2 v(z)\mathrm{d}z, \tag{5}$$

where ω is the angular speed of oscillation ($\omega = 2\pi f$, where f is stimulus frequency), F_m is the inertial force, v is cupular deflection, and ρ_m is the density of the cupular matrix.

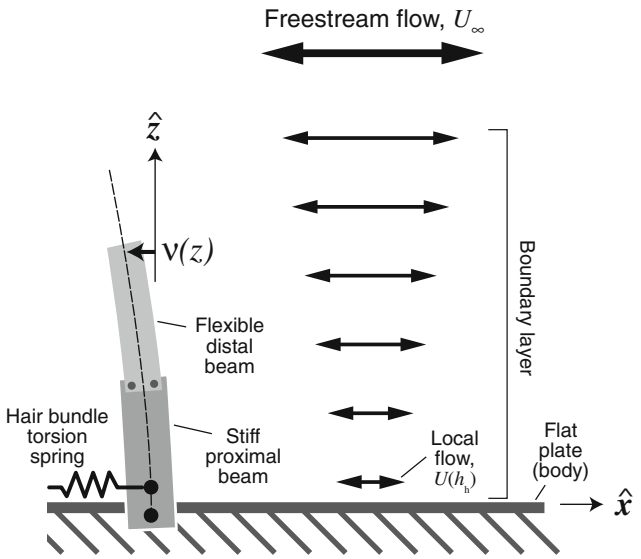

Fig. 2 The fluid–structure interaction model of a superficial neuromast. The cupula is modeled as a two-part beam excited by a pressure-driven oscillating boundary layer. Deflections, $v(z)$, were calculated over a range of stimulus frequencies. The juncture between the cupula and the sensory epithelium is modeled as a pivot and spring to simulate the torsion stiffness generated by the hair bundles

Hydrodynamics

The model treats the stimulus as an oscillating pressure field and calculates its boundary layer over a flat surface. The flow velocity of the boundary layer varies with distance from the surface according to the following function (Batchelor 1967):

$$U(z) = U_\infty\left(1 - \exp\left(\frac{-z(1+i)}{\delta}\right)\right), \tag{6}$$

where U_∞ is the freestream velocity, and δ is the boundary layer thickness. This is calculated with the following equation (Batchelor 1967):

$$\delta = \sqrt{\frac{2\mu}{\rho_w \omega}}, \tag{7}$$

where ρ_w and μ are, respectively, the density and dynamic viscosity of water.

The model of fluid forces acting on the cupula was based on the flow that develops around a uniform cylinder in oscillating flow. Such flow generates both viscous and inertial forces on the surface of the cylinder. The viscous drag, F_u, on an element of the cylinder is given by (Stokes 1851):

$$F_u(z) = 4\pi\mu k(U(z) - i\omega v(z))\mathrm{d}z, \tag{8}$$

where v is the deflection of the cupula, and k is a viscous drag coefficient. The viscous drag coefficient is calculated as follows (Stokes 1851):

$$k = -\frac{L}{L^2 + (\pi/4)^2}. \tag{9}$$

Under the assumption that $k \ll 1$, L may be calculated as (Stokes 1851):

$$L = \gamma + \ln\left(\frac{a}{\sqrt{2\delta}}\right), \tag{10}$$

where γ is Euler's constant ($\gamma \approx 0.5772$). The relative acceleration of the flow and the cupula results in a second force, the acceleration reaction, F_a, that can be calculated as (Stokes 1851):

$$F_a(z) = \left(\pi\rho_w a^2 - \frac{\pi^2\mu k}{\omega L}\right)\left(i\omega U(z) + \omega^2 v(z)\right)\mathrm{d}z, \tag{11}$$

Lastly, the pressure field that develops around the cupula as the flow accelerates results in a buoyant force, F_b, that may be calculated as:

$$F_b(z) = i\rho_w \pi a^2 \omega U(z)\mathrm{d}z. \tag{12}$$

These equations rely on some simplifying assumptions. Stokes' (1851) treatment of an oscillating pendulum in fluid assumes a rigid cylinder with a circular cross-section. These hydrodynamics focus exclusively on the two-dimensional flow field around the cross-section of an infinitely long cylinder and therefore neglect forces that may be generated by gradients in pressure or shear stress along the cylinder's height. This blade-element approach has been applied to modeling the rigid filiform hairs of insects in both air and water (Humphrey et al. 1993; Devarakonda et al. 1996). However, it is unclear if the same approach comprehensively describes the hydrodynamics of less elongated structures. Studies on the hydrodynamics of protuberances with an aspect ratio comparable to a cupula (the height is about four times its base diameter, Van Trump and McHenry 2008) have not explicitly examined the role of height-wise gradients (e.g. Pozrikidis 1997; Shatz 2005). Therefore, our blade-element approach should be regarded as a first-order approximation of the hydrodynamics of a cupula.

Stokes' (1851) further assumes that viscous forces dominate and the inertia of the freestream flow may be neglected. This approximation has been verified for particular hydrodynamic regimes in previous studies. These regimes are expressed by the dimensionless Reynolds number, Re, and Strouhal number, St, both of which vary with height in our model because of the boundary layer over the body:

$$Re = \frac{2a\rho_w}{\mu}|U(z)|, \tag{13}$$

$$St = \frac{a\omega}{|U(z)|}. \tag{14}$$

When $Re < 1$, the hydrodynamics of a cylinder are dominated by viscous forces. In accordance with Stokes' assumptions, when $0.1 < St < 100$, the inertia of the freestream flow has been confirmed to play only a minor role (Stuart 1963; Hussey et al. 1967; Williams and Hussey 1972; Sarpkaya 1986). Thus, in this range of Strouhal numbers, the Oseen correction (Oseen 1910; Lamb 1911, 1945) may be neglected and the Stokes solution applies. Our model remains within this regime for a particular range of freestream velocities. At high frequencies, the freestream velocity must remain high enough that $St < 100$. This velocity may be calculated by substituting the boundary layer equation (Eq. 6) into the St equation (Eq. 14) as: $U_\infty > a\omega/(100|1 - \exp(-z(1+i)/\delta)|)$. This suggest that at the height $z = 5$ μm, which is relatively close to the body, the freestream velocity should exceed a value of 0.9 mm s^{-1} for a typical superficial neuromast ($a = 5$ μm) at $f = 1{,}000$ Hz. At low frequencies, the St values in the distal region are relatively low. Combining Eqs. 6 and 14 for $St > 0.1$ yields the following inequality: $U_\infty < 10a\omega/|1 - \exp(-z(1+i)/\delta)|$. This suggest that at a height of $z = 35$ μm, near the distal tip of the cupula in zebrafish (McHenry and van Netten 2007), the freestream velocity should be less than 0.9 m s^{-1} at $f = 0.1$ Hz.

However, combining Eqs. 6 and 13 and solving for $Re < 1$ yields: $U_\infty < \mu/(2a\rho|1 - \exp(-z(1 + i)/\delta)|)$, which suggests that $U_\infty < 0.3$ m s^{-1}. Therefore, the hydrodynamics assumed by Stokes (1851) have been verified for conditions where the freestream flow remains within the following range: 0.9 mm s^{-1} $< U_\infty <$ 0.3 m s^{-1}. For comparison, a larval zebrafish may swim at speeds below 1 mm s^{-1} (McHenry and Lauder 2005) and the flow generated by a predator fish may reach velocities up to 0.6 m s^{-1} (Higham et al. 2006). Therefore, the extremes of biologically relevant velocities may fall outside the bounds of hydrodynamics assumed by our model that have been verified by prior experimentation (Stuart 1963; Hussey et al. 1967; Williams and Hussey 1972; Sarpkaya 1986).

The governing equation

The net force acting on an element of the cupula is the sum of structural and hydrodynamic forces. This sum is given by the following equation:

$$F_e(z) + F_m(z) = F_u(z) + F_a(z) + F_b(z). \tag{15}$$

Substituting from Eqs. 4, 5, 8, 11 and 12 yields the following relationship:

$$EIv''''(z) = i\omega b_m v(z) - b_w U(z), \tag{16}$$

where

$$b_m = -4\pi\mu k - i\pi(\rho_m + \rho_w)a^2\omega + \frac{i\pi^2\mu k}{L}$$

and

$$b_w = -4\pi\mu k - 2i\pi\rho_w a^2\omega + \frac{i\pi^2\mu k}{L}.$$

For a beam of uniform stiffness along its length, we found the general solution to this equation to be:

$$v(z) = -\frac{ib_w U_\infty}{\omega b_m}\left[1 - \frac{i\omega b_m \delta^4}{4EI + i\omega b_m \delta^4}\exp\left(\frac{-(1+i)z}{\delta}\right)\right] + \sum_{j=0}^{3} C_j \exp\left(i^j z\sqrt[4]{\frac{i\omega b_m}{EI}}\right), \tag{17}$$

where C_j is a sequence of four integration constants. This solution describes the deflections of each of the two beams of the cupula model (Fig. 2).

Formulating a specific prediction for the deflection of a cupula requires defining the conditions at the ends of the two beams. At the very tip of the distal beam, the cupula lacks any height or area for fluid forces to be generated. Therefore, one may assume that there is no bending moment ($EIv_2''(h_c) = 0$) or shear force ($EIv_2'''(h_c) = 0$) at this position (Fig. 2). The two parts of the cupula are made consistent where they intersect by matching their deflection ($v_1(h_k) = v_2(0)$), orientation ($v_1'(h_k) = v_2'(0)$), bending moment ($(EI)_1 v_1''(h_k) = (EI)_2 v_2''(0)$), and shear force ($(EI)_1 v_1'''(h_k) = (EI)_2 v_2'''(0)$). Finally, the cupula was assumed pinned at the base ($v(0) = 0$) and the hair bundles were modeled as a torsion spring that resists changes in orientation at the base of the proximal cupula. This stiffness is generated in a hair cell by the anchoring of the kinocilia and their linkage to the stereocilia (Hudspeth and Corey 1977; Hudspeth and Jacobs 1979; Hudspeth 1989). This stiffness was set equal to the product of the number of hair cells, N, and hair bundle torsional stiffness, q_t:

$$v'(0) = \frac{(EI)_1 v''(0)}{Nq_t}, \tag{18}$$

where the product $(EI)_1 v''(0)$ is equal to the total bending moment acting on the base of the cupula.

Specific predictions of cupular deflection were calculated from the general solution to the governing equation. The eight integration constants for the two beams were calculated using the boundary conditions prescribed above. These boundary conditions provided eight simultaneous linear equations that were solved numerically to find values for all integration constants of the general solution (Eq. 18). Since the cupula of a superficial neuromast bends in flow (Schulze 1861; Cahn and Shaw 1962; Dinklo 2005), it is necessary to examine cupular deflection at a particular height. Unless otherwise noted, we chose to evaluate cupular deflections at the height of the tip of the tallest stereocilium because of its close proximity to the site of mechanotransduction (Hudspeth 1982). Normalizing this deflection with respect to the freestream velocity provides a measure of sensitivity that is independent of stimulus intensity. Therefore, we calculated neuromast sensitivity as the following ratio:

$$S_f = \frac{v(h_h)}{U_\infty}, \tag{19}$$

where h_h is the height of the tip of the stereocilia ($h_h = 5.2$ μm in zebrafish) (Dinklo 2005). This measure of sensitivity has real and imaginary components, and provides information about both the degree and timing of the cupular deflection with respect to the freestream flow. The amplitude and phase of this response were, respectively, calculated as the modulus and argument of sensitivity with the amplitude having units of time ($s = \text{m}(\text{m s}^{-1})^{-1}$), as in van Netten (2006). The viscous component of the cupular material has yet to be measured in zebrafish. We therefore treated the cupular matrix as a purely elastic material with a complex modulus equal to its Young's modulus ($E = E' = 21$ Pa, McHenry and van Netten 2007). For model validation and analysis, we focused on the superficial neuromasts of zebrafish larvae, *Danio rerio*, using

Table 1 Parameter values for neuromasts of zebrafish larvae

Parameter	Value	Source
a (μm)	4.44	Dinklo (2005)
E_m (Pa)	21	McHenry and van Netten (2007)
$(EI)_k$ (N m^2)	2.4×10^{-21}	McHenry and van Netten (2007)
h_b (μm)	5.2	Dinklo (2005)
h_c (μm)	45.0	Dinklo (2005), McHenry and van Netten (2007)
h_k (μm)	16.0	McHenry and van Netten (2007)
N	10	Dinklo (2005)
q_l (N m^{-1})	1.3×10^{-3}	van Netten and Kroese (1987)
q_t (Nm rad^{-1})	2.9×10^{-14}	van Netten and Kroese (1987)
μ (Pa s)	0.7975×10^{-3}	Weast (1987)
ρ_m (kg m^3)	996	$\rho_m = \rho_w$
ρ_w (kg m^3)	996	Weast (1987)

a, radius of cupula; E_m, Young's modulus of cupular matrix; $(EI)_k$, flexural stiffness of kinocilium, h_b, height of hair bundle; h_c, height of cupula; h_k, height of kinocilia; N, number of hair cells; q_l, linear spring stiffness; q_t, torsion spring stiffness; μ, dynamic viscosity of water; ρ_m, density of cupular matrix; ρ_w, density of water

parameter values (Table 1) for that species. A frequency response for sensitivity was calculated by finding solutions to the general solution (Eqs. 18, 20) numerically for hundreds of frequencies between 0.01 and 1,000 Hz. In a sensitivity analysis, individual parameter values were varied in multiple simulations between realistic lower and upper parameter values. The frequency responses of simulations were compared by calculating their maximum amplitude and cut-off frequency. Cut-off frequency was approximated as the frequency at which the maximum amplitude occurred.

The frequency response to a vibrating sphere

The frequency response of a superficial neuromast to a vibrating sphere was also considered through a modification of our mathematical model. A vibrating sphere is commonly used as a stimulus for behavioral and neurobiological experimentation in lateral line research. We therefore used Stokes (1851) treatment of the flow generated by an oscillating sphere, which considers viscous hydrodynamics in the near field. At a distance r from the center of the sphere, in a direction perpendicular to the sphere's motion, this model predicts flow velocity parallel to the motion of the sphere to be given by (based on Eq. 29 in van Netten 2006):

$$U_s(z) = -\frac{3a_s W}{2r}\left[1 + \frac{(1-i)\delta}{2r} - \frac{1\delta^2}{2r^2}\right] \exp\left[\frac{-(1+i)(r-a_s)}{\delta}\right] + \frac{3a_s^3 W}{2r^3}\left[\frac{1}{3} + \frac{(1-i)\delta}{2a_s} - \frac{1\delta^2}{2a_s^2}\right], \quad (20)$$

where W and a_s are the velocity and radius of the sphere, respectively. This model neglects the acoustic pressure wave that dominates flow in the far field at higher frequencies. To evaluate this assumption for superficial neuromasts, we compared the frequency responses predicted by Eq. 20 with a model that considers both fluid compressibility (far field) and viscosity (near field) (art. 361 in Lamb 1911). The magnitude of the acoustic effect increases with frequency, distance from the sphere, and the sphere's radius. Yet, we found that this effect remains negligible even at parameter values (e.g. $f = 2$ kHz, $r = 100$ mm, and $a_s = 5$ mm) beyond the range that is typically used in behavioral (e.g. Coombs and Conley 1997) or physiological (e.g. Kroese and Schellart 1987) studies. We therefore conclude that the viscous hydrodynamics of an oscillating sphere (Eq. 20) dominate the flow detected by superficial neuromasts under experimental conditions.

We have approximated the flow field generated by a sphere oscillating near a flat plate with the method of mirror images. This approach approximates the hydrodynamics between a sphere and a flat plate by modeling the flow generated between two spheres oscillating in antiphase. This approximation relies on two assumptions. The components of velocity that are parallel to the bisecting plane cancel and thereby obey the no-slip condition. However, the component of the velocity that is normal to the plane sums. Thus, the calculated flow field is a solution for the case in which the plate bends slightly with the flow rather than remaining perfectly flat. Second, this approach requires that the displacement of the sphere is small relative to the distance p between the sphere and the plate (i.e. $2\pi U_s/\omega \ll p$). When this displacement is small, the positions along the plate are almost equidistant to both spheres and the velocities cancel at the plate. Under these assumptions, the flow is given by:

$$U_{s,mir}(z) = U_s(p - z) - U_s(p + z), \quad (21)$$

where z is the height from the surface of the plate. To more easily examine how the flow acts on the cupula, we

calculated a linear expansion of Eq. 21, which is valid in the vicinity of the flat plate:

$$U_{s,lin}(z) = -\frac{3a_s Wz}{\delta p}\left[(1+i)+\frac{2\delta}{p}+\frac{3(1+i)\delta^2}{2p^2}-\frac{3i\delta^3}{2p^3}\right] \times \exp\left[-\frac{(1+i)(p-a_s)}{\delta}\right] + \frac{3a_s^3 Wz}{p^4}\left[1+\frac{3(1-i)\delta}{2a_s}-\frac{3i\delta^2}{2a_s^2}\right] \quad (22)$$

where $z/\delta \ll 1$ and $x/p \ll 1$. The sensitivity S_l of local flow at the stereocilia height was calculated with respect to the sphere's velocity ($S_l = U_{s,lin}(h_h)/W$) to relate its frequency response to that of the cupula. The hydrodynamics of a sphere oscillating near a plate have been treated more comprehensively in prior studies (Wakiya 1961; Wakiya 1963).

The boundary layer generated by a sphere is well approximated by a linear function of height [$U(z) = \beta z$; cf. Eq. 22]. We found the general solution to the governing equation of our cupula model using this linear boundary layer profile [$U(z) = U_{s,lin}(z)$ in Eq. 16] instead of the nonlinear profile used to find the general solution for pressure-driven flow (Eq. 17). The following equation describes the solution to the cupula model (Eq. 16) for such a boundary layer:

$$v_s(z) = -\frac{ib_w\beta}{\omega b_m}z + \sum_{j=0}^{3} C_j \exp\left(i^j z\sqrt[4]{\frac{i\omega b_m}{EI}}\right). \quad (23)$$

The sequence of integration constants C_j was solved for using the same boundary conditions as for pressure-driven flows and the sensitivity S_s of cupular deflections to the sphere was again calculated as $S_s = v_s(h_h)/W$.

Results

The model predicts that the boundary layer and mechanics of the cupula behave as a band-pass filter of freestream flow. Sensitivity, defined as the ratio of cupular deflection to freestream velocity (Eq. 19), increases at low frequencies at a rate of 12 dB dec^{-1} and attenuates at high frequencies with a rate around −15 dB dec^{-1} (Fig. 3a). The maximum amplitude and the cut-off frequency depend on cupular morphology and the height at which deflections are evaluated.

Model validation

The model was tested by comparing its predictions with measurements of cupular deflections in the superficial neuromasts of zebrafish larvae (Dinklo 2005). We chose a value for cupular height ($h_c = 33$ μm) within the range for the species (Van Trump and McHenry 2008) that matched the measured maximum amplitude of sensitivity (Fig. 3a) because this parameter was not reported with the deflection measurements. Although these adjustments prohibit an evaluation in terms of absolute values, the form of the

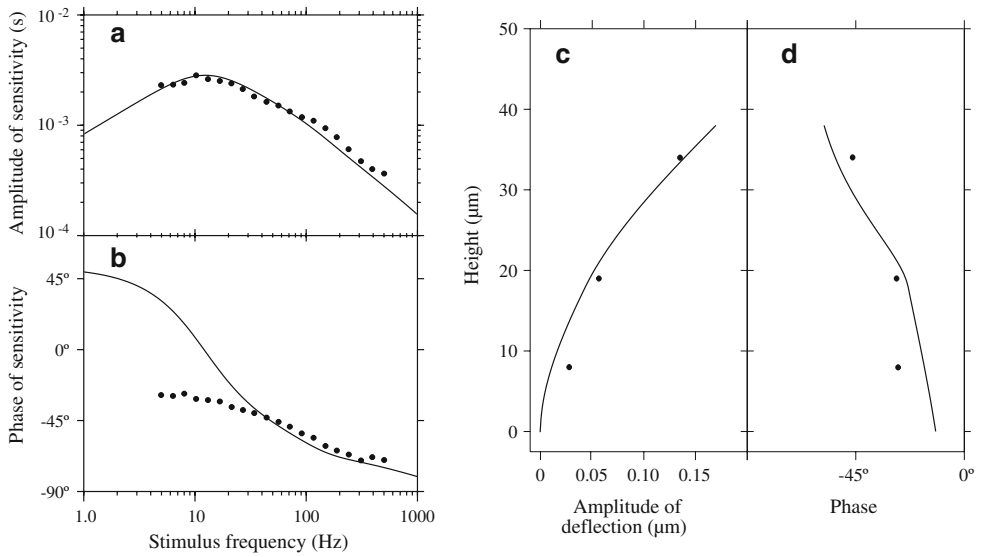

Fig. 3 Model predictions compared with measured deflections in zebrafish larvae. The measurements of Dinklo (2005) (*filled circles*) are overlaid on the prediction of the model (*solid curve*) for the same conditions. The predictions of the model are shown with the standard parameter values (Table 1), except cupular height: $h_c = 33$ μm. Measurements of the **a** amplitude ($|S_f|$), and **b** phase (180° arg(S_f)) of sensitivity with respect to the freestream flow are shown for $z = 29$ μm. **c** The amplitude ($|v(z)|$) and **d** phase (180° arg($v(z)/U_\infty$)/π) of the cupula at three heights ($z = 8$ μm, $z = 19$ μm, and $z = 34$ μm) for a stimulus frequency of $f = 44.0$ Hz. The stimulus amplitude was adjusted to $U_\infty = 11.4$ μm s^{-1} to match the data in **c** and **d**

measured frequency response shows good agreement with the model in the amplitude of sensitivity (Fig. 3a). Measured phase also agreed with the model at frequencies above 30 Hz (Fig. 3b), but diverged at lower frequencies, where the model predicts a phase around 45°. That the measurements reflect a phase closer to −30° at low frequencies may be attributed to a difference between the discrete fluid jet stimulus in Dinklo's (2005) experiments and the fluid velocity field assumed by our model (Eq. 6).

Our model predicts a similar profile of cupular deflection with height as was measured in zebrafish neuromasts. Dinklo (2005) measured deflection at three different heights along the cupula for a single stimulus frequency (Fig. 3c, d). For comparison with these measurements, the freestream flow was adjusted to 11.4 μm s^{-1} such that the magnitude of deflection approximated the data. Although this freestream velocity is slower than the range for which the model's hydrodynamics have been validated (Stuart 1963; Hussey et al. 1967; Williams and Hussey 1972; Sarpkaya 1986). The model predicts cupular bending that is similar to measurements (Dinklo 2005) and previous observations (Schulze 1861; Cahn and Shaw 1962).

Effects of cupular morphology on the frequency response

We used a sensitivity analysis to test the effects of the hair cells on the frequency response of the cupula. Varying the torsion spring stiffness of the hair bundles (Fig. 2) showed little effect on cupular sensitivity unless reduced to an unrealistically small level (Fig. 4ai–ci). Hair cells influence cupular mechanics by contributing kinocilia to the flexural stiffness of the cupula. This is demonstrated by the similar effect of the number of hair cells and kinocilium flexural stiffness on maximum amplitude and cut-off frequency (Fig. 4aii–cii, aiii–ciii). Cupulae with taller kinocilia exhibit greater sensitivity up to the point where kinocilia height approaches that of the cupula (e.g. $h_k = 30$ μm in a 45 μm cupula, Fig. 4aiv).

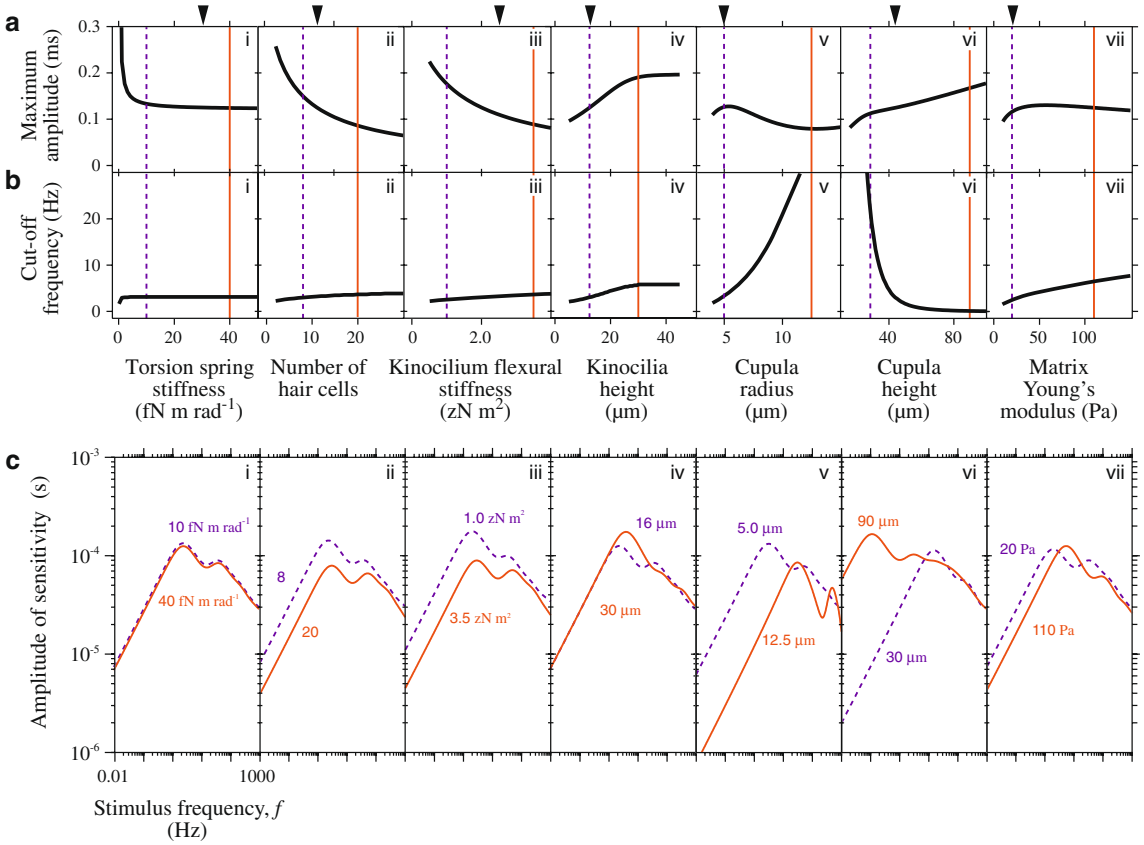

Fig. 4 Sensitivity analysis of the effects of morphology and mechanical properties on the frequency response of the cupula with a pressure-driven stimulus at the stereocilia height (5.2 μm). Differences in maximum amplitude **a** and cut-off frequency **b** of sensitivity (S_f, Eq. 19) are shown as a function of each morphological and mechanical parameter in the model. Individual parameters were varied with all other parameters held constant at the values for zebrafish larvae (Table 1), which are denoted by the *arrowheads* above each *panel*. **c** The amplitude ($|S_f|$) of the frequency response for high (*orange*) and low (*dashed purple*) values for the parameter varied in **a** and **b**

The dimensions of the cupular matrix affect a superficial neuromast's frequency response by influencing structural mechanics and hydrodynamics. A wider cupula causes the maximum amplitude of sensitivity to decrease for an increase in cupula radius above 6 μm (Fig. 4av). In contrast, there is a monotonic increase in sensitivity with increases in cupula height over the range that we examined (Fig. 4avi). However, the influence of cupula height is mediated by the material composition of the cupular matrix (Fig. 4avii–cvii).

The role of the hair bundles in the dynamics of the cupula was further considered by comparing simulations that differed by the coupling between the cupula and body (Fig. 5). The boundary conditions of the model were modified by replacing the pivoting base (Eq. 18) with a zero angle of orientation at the base of the cupula

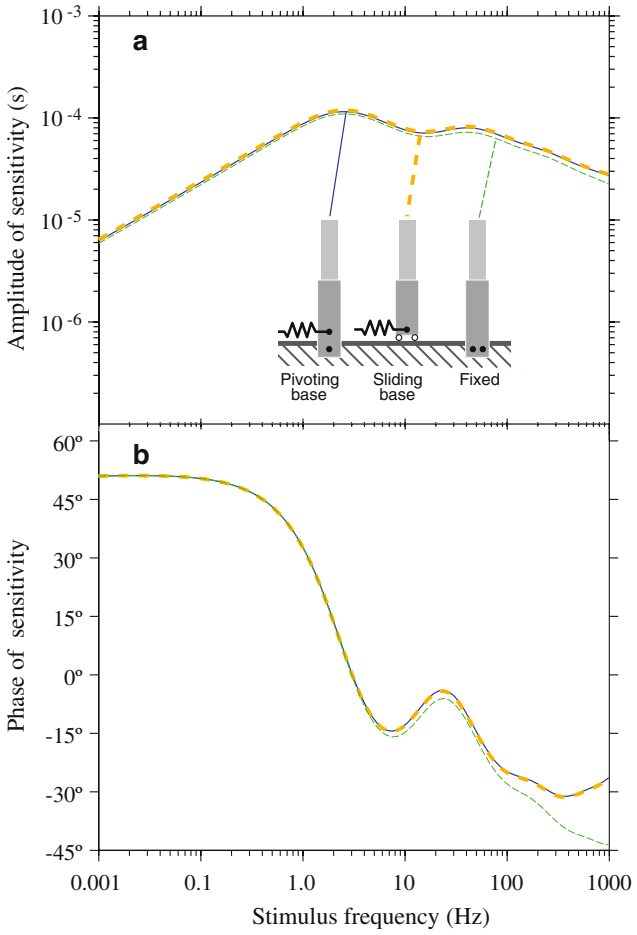

Fig. 5 The frequency response with a pressure-driven stimulus for three different models of the juncture between the cupula and body. Each *curve* represents a prediction of the model under different boundary conditions using parameter values for zebrafish larvae (Table 1). Each prediction is shown in terms of the **a** amplitude ($|S_f|$) and **b** phase ($180° \arg(S_f)/\pi$) of sensitivity (Eq. 19). The pivoting base (*solid blue*, Fig. 2), sliding base (*thick dashed orange*), and fixed base (*thin dashed green*)

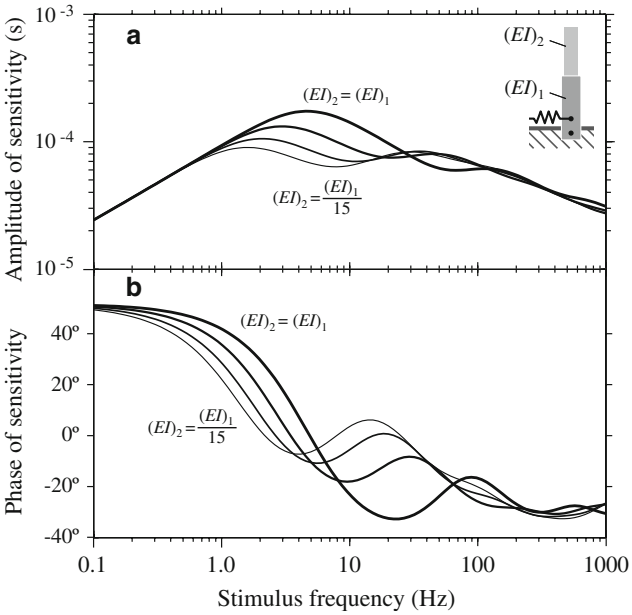

Fig. 6 Influence of the flexural stiffness of the distal tip of the cupula on the frequency response. The four simulations differ in the flexural stiffness of the distal region of the cupula $(EI)_2$ relative to the proximal region $(EI)_1$: $(EI)_2 = (EI)_1$, $(EI)_2 = (EI)_1/5$, $(EI)_2 = (EI)_1/10$, and $(EI)_2 = (EI)_1/15$. The **a** amplitude ($|S_f|$) and **b** phase ($180° \arg(S_f)/\pi$) of sensitivity to freestream flow are shown for each value of distal stiffness

($v'(0) = 0$) and resisting sliding with a linear spring ($v(0) = EIv'''(0)/nq_l$, where q_l is linear stiffness, Table 1). The frequency response predicted for these conditions did not differ greatly from the pivoting base (Fig. 5; orange curve) or when both rotation and translation were fixed at zero (Fig. 5a; orange curve). The only substantial discrepancies occurring in phase at higher frequencies ($f > 100$ Hz, Fig. 5b), where the neuromasts are relatively insensitive (Fig. 5a).

The functional consequences of a flexible distal tip were examined by comparing the predictions of different simulations. Simulations using flexural stiffness greater than what was observed ($(EI)_2 \approx (EI)_1/15$; McHenry and van Netten 2007) predicted higher maximum amplitude in sensitivity and a higher cut-off frequency (Fig. 6). Therefore, the composition of the matrix material that comprises the tip of the cupula has a substantial influence on the frequency response.

Frequency response with a sphere stimulus

A cupula is most sensitive to the oscillations of a sphere at low frequencies (Fig. 7). For a sphere of small radius (e.g. $a_s = 1$ mm), sensitivity attenuates at a rate of ~ -15 dB dec^{-1} throughout the frequency range considered. The same trend is predicted at higher frequencies ($f > 10$ Hz) for spheres of larger radius. However, these

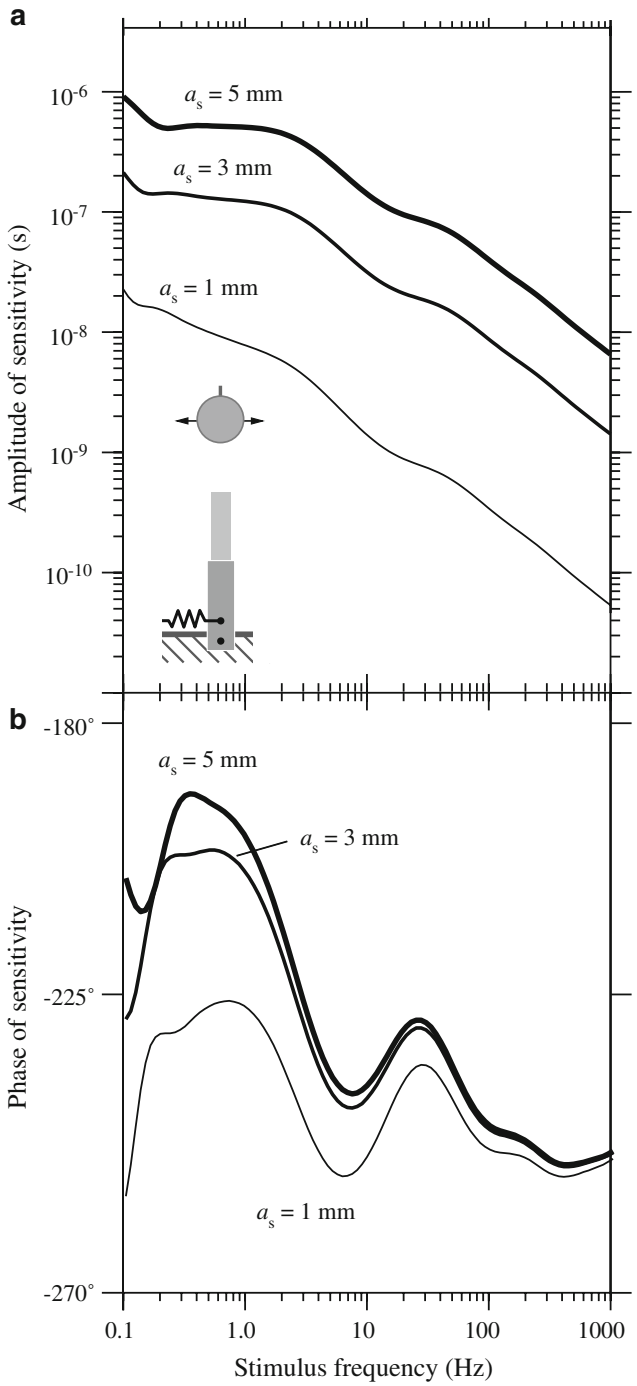

Fig. 7 Frequency response of the cupula to an oscillating sphere. The amplitude **a** and phase **b** of cupular sensitivity (S_s) are shown. *Curves* of greater thickness correspond to responses from spheres of larger radius a_s. Assumptions about the hydrodynamics of the cupula are violated at $f < 0.1$ Hz and therefore are not presented. All simulations used the mean parameter values for zebrafish larvae (Table 1)

larger spheres also exhibit a flat response for a range of lower frequencies (e.g. 0.2 Hz $< f <$ 2 Hz for $a_s = 5$ mm, Fig. 7a). None of the frequency responses with a sphere exhibit the low-frequency attenuation predicted for pressure-driven flow (Fig. 5).

Discussion

Filtering by the boundary layer

Well-established hydrodynamic theory suggests that the boundary layer over the surface of a fish's body plays a major role in determining the signals detected by a superficial neuromast (Batchelor 1967; Schlichting 1979). Boundary layer thickness, and therefore signal attenuation, reduces with increasing stimulus frequency and therefore exposes a neuromast to more rapid flow (Fig. 8). These changes in the boundary layer with frequency are reflected in the sensitivity S_b of local flow (the velocity at the stereocilia height $U(h_h)$, Fig. 2) to freestream flow ($S_b = U(h_h)/U_\infty$, Eq. 6). The amplitude of this sensitivity increases with frequency at a rate of 10 dB dec^{-1} (Fig. 9a) and creates a 45° phase lead of local flow (Fig. 9b). This filtering influences the response over all frequencies considered and dominates changes in the amplitude and phase shift of cupular deflections at low frequencies ($f < 1.0$ Hz in Fig. 9a).

The frequency response of a cupula is different when stimulated by a vibrating sphere. The boundary layer between a sphere and the body's surface may be considered by normalizing local flow to the velocity of the sphere ($S_l = U_{s,lin}(h_h)/W$, Eqn. 20). This measure of sensitivity exhibits a two-gain frequency response with greater attenuation at higher frequencies than at lower frequencies (Fig. 10). This frequency response contrasts the high-pass filtering of a pressure-driven boundary layer (Fig. 9) and may be understood by examining its profile (Fig. 11). At low frequencies, the sphere viscously carries a large volume of fluid and the amplitude of velocity near the body's surface is consequently large (e.g. $f = 0.1$ Hz in Fig. 11b, c). At high frequencies, the flow generated by the sphere saturates to an irrotational dipole field (e.g. $f = 100$ Hz, Fig. 11d, e) with an amplitude that varies with distance to the sphere as a^3/r^3 (i.e. the second term of Eqn. 20 dominates). Therefore, the flows that excite a cupula are determined by the boundary layer hydrodynamics of both the sphere and the body's surface.

This consideration of the viscous flows generated by a sphere is a departure from many prior studies on the lateral line system. The flow field generated by a vibrating sphere can be calculated using a simple dipole model if the flow is assumed to be inviscid and irrotational (Denton and Gray 1983; Denton and Gray 1982; Kalmijn 1988; Kalmijn 1989; Bergeijk 1967). This inviscid theory successfully predicts the microphonic and afferent potentials generated by canal neuromasts (Coombs et al. 1996; Coombs and

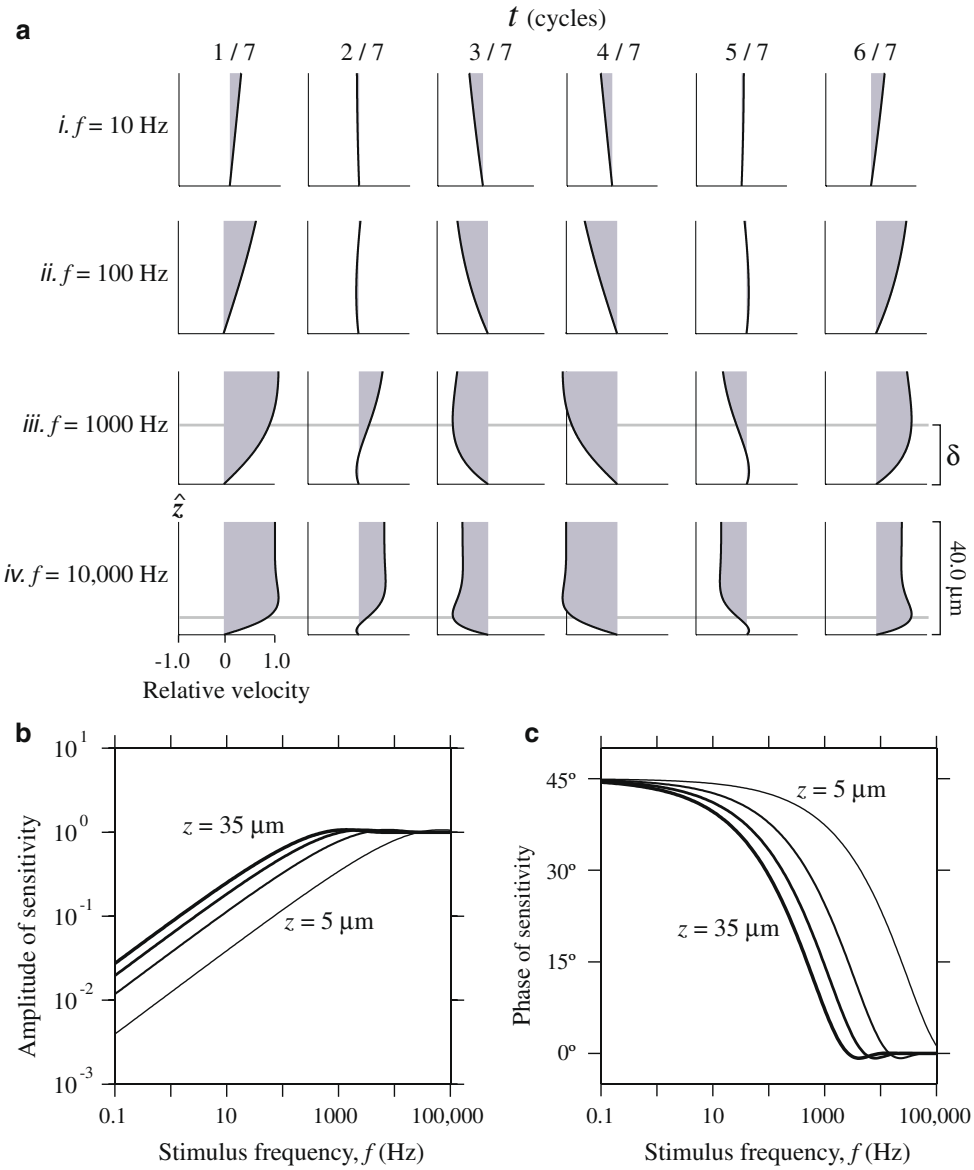

Fig. 8 Profile of a pressure-driven oscillatory boundary layer over a flat plate. All *plots* illustrate the velocity of flow within the boundary layer (Eq. 6), relative to the freestream velocity, U_∞. **a** The boundary layer velocity profile (*gray field*) along the height (z) from a flat plate, over time (t). The *gray line* denotes boundary layer thickness δ. **b** The amplitude and **c** phase of flow relative to the stimulus are shown for heights of 5, 15, 25 and 35 µm with *thicker curves* correspond to greater height

Conley 1997; Curcic-Blake and van Netten 2006), but fails to model the boundary layers to which superficial neuromasts are exposed (Kuiper 1967; Daniel 1981; Hassan 1985; Kalmijn 1988; Teyke 1988; Anderson et al. 2001; Dinklo 2005). Therefore, the present approach, which is consistent with van Netten (2006) and previously suggested by Kalmijn (1988), is more appropriate for the signals detected by superficial neuromasts than prior models.

These findings have implications for neurophysiological experiments on superficial neuromasts. The form of the reported frequency responses (e.g. Kroese and Schellart 1987; Montgomery and Coombs 1992; Münz 1985; Kroese et al. 1980; Harris and Milne 1966) varies among neurophysiological studies and some investigators using similar techniques have reached conclusions differing from the consensus view (e.g. Kroese et al. 1978; Münz et al. 1984). As demonstrated by our results and previously suggested (Kroese and Schellart 1987; Kalmijn 1988), some of these discrepancies may be attributed to filtering by the boundary layer. For example, frequency responses vary greatly with the diameter (Fig. 7) and position (Fig. 10) of a vibrating sphere. Therefore, measurements of frequency response may vary with small differences in an experimental setup.

Frequency response measurements may be examined independent of filtering by the boundary layer. The sensitivity of cupular deflection to local flow exhibits a similar frequency response regardless of the stimulus source. This is revealed by the similar responses with pressure-driven flow (S_h, thin line in Fig. 9) to those with an oscillating sphere (S_s, thin line in Fig. 10). Sensitivity defined with respect to local flow allows an examination of filtering by a neuromast without the confounding influence of the

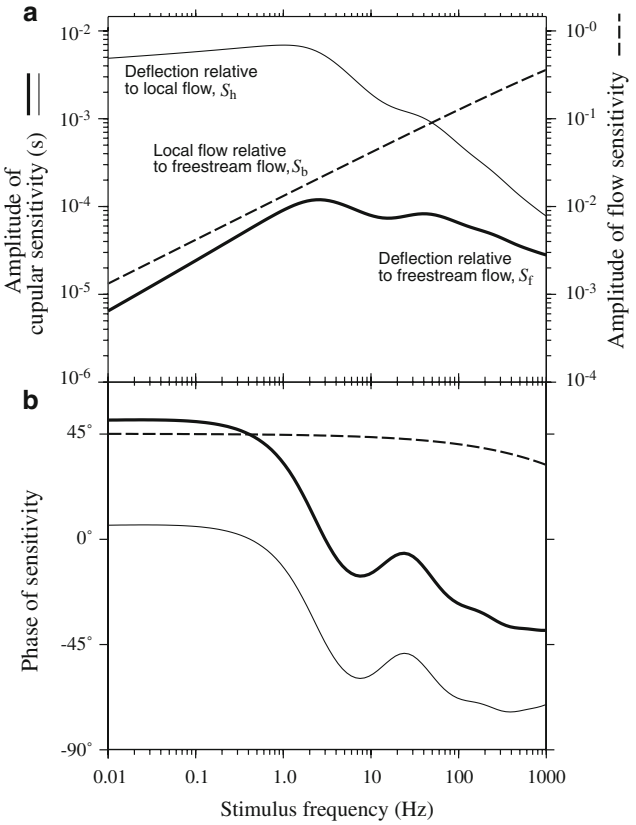

Fig. 9 Influence of a pressure-driven boundary layer on the frequency response. The amplitude **a** and phase **b** of different measures of sensitivity are shown for the same simulation of zebrafish larvae (parameter values in Table 1). The sensitivity of the cupula to freestream flow, S_f (*thick curve*), includes the influence of the boundary layer. The frequency response predicted for the cupula's sensitivity to local flow, S_h (*thin curve*) does not include the filtering of the flow stimulus by the boundary layer. The difference between these curves equals the sensitivity of local flow induced by the freestream flow S_b (*dashed curve*)

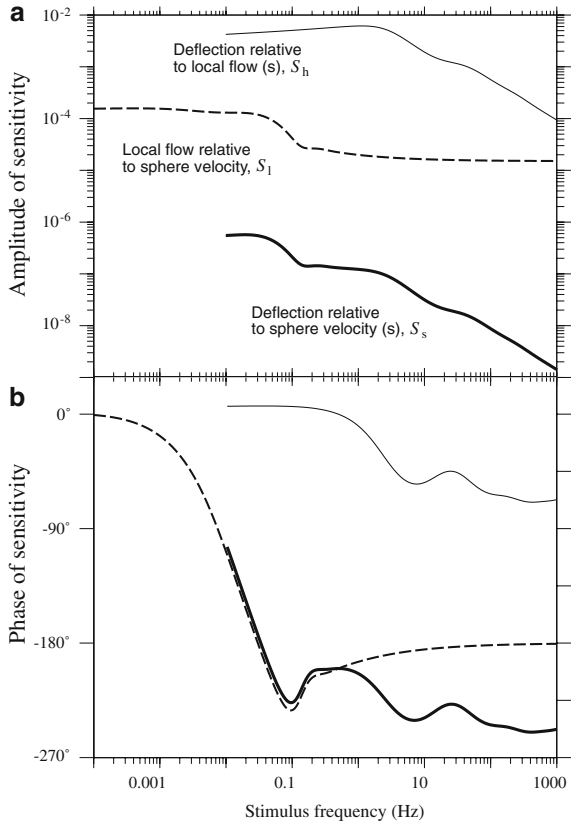

Fig. 10 Influence of the boundary layer on the frequency response with a vibrating sphere stimulus. The amplitude **a** and phase **b** of different measures of sensitivity are shown for the same simulation (parameter values in Table 1) with a vibrating sphere as the stimulus. The sensitivity of the cupula to the velocity of the sphere S_s (*thick curve*), includes the influence of the boundary layer. The frequency response predicted for the cupula's sensitivity to local flow, S_h (*thin curve*) does not include the filtering of the flow stimulus by the boundary layer. This filtering by hydrodynamics is reflected in the sensitivity of local flow to sphere velocity S_l (*dashed curve*)

boundary layer, but requires a model (e.g. Eq. 6 or 22) or measurement of local flow.

Filtering by fluid–structure interaction

The cupula exhibits a nearly flat (2 dB dec^{-1}) response in amplitude (Figs. 9a, 10a) and a phase (Figs. 9b, 10b) to the local flow velocity at low frequencies (Figs. 9, 10). This suggests that a superficial neuromast encodes the velocity of flow close to the body with low-pass filtering. Therefore, the band-pass frequency response of a superficial neuromast to pressure-driven flow (Figs. 3, 4, 5, 6) is generated by the combination of low-pass filtering by the fluid–structure interaction of the cupula and the high-pass filtering by the boundary layer (Fig. 9). The low-pass filtering of the cupula combines with the two-gain filtering of the boundary layer to determine the frequency response with a vibrating sphere stimulus (Fig. 10).

The frequency response of a superficial neuromast to local flow may be understood by considering the forces acting on the cupula. At low frequencies (e.g. $f = 1$ Hz), viscous drag dominates the forces acting on the cupula (Fig. 12ai). This viscous coupling causes the cupula to deflect in proportion to (Figs. 9a, 10a), and in phase with (Figs. 9b, 10b) local flow. At higher frequencies (e.g. $f = 100$ Hz), acceleration reaction acts to accelerate the cupula with the surrounding water (Fig. 12bi). Therefore, cupular deflections become closer to deflecting in proportional to, and in phase with, the displacement of the water at higher frequencies. Therefore, the frequency response of the cupula is due to changes in the relative magnitude of hydrodynamic forces with frequency.

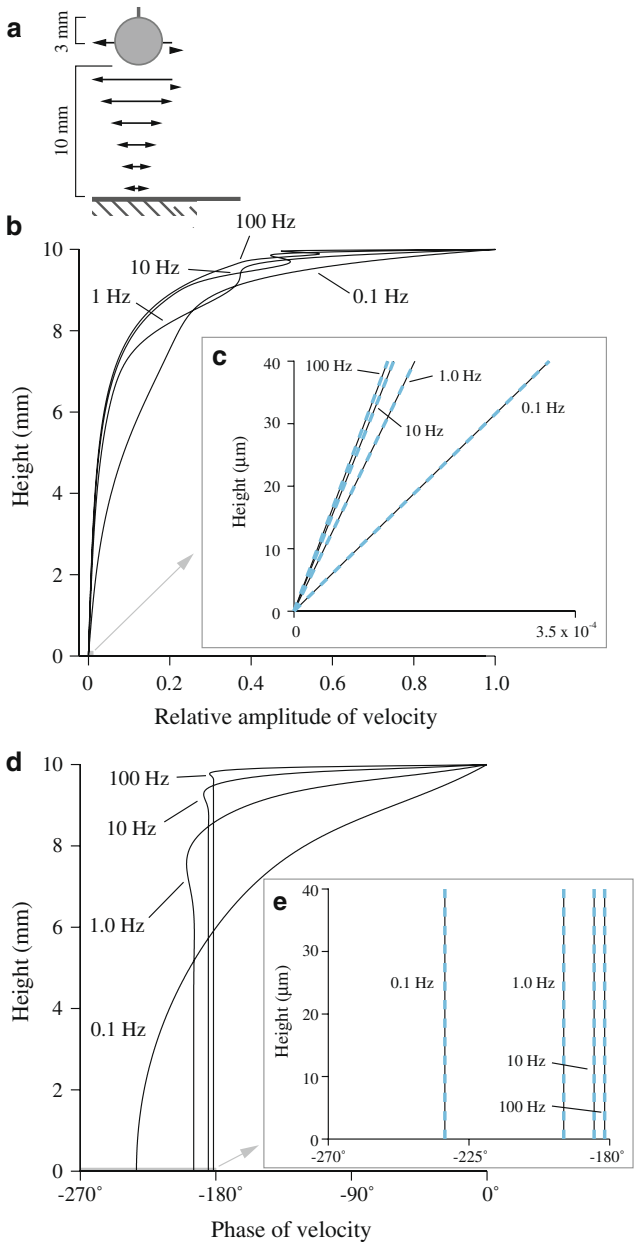

Fig. 11 Flow generated by a sphere oscillating along a flat plate. **a** Schematic of the flow (*black curves*) generated by a sphere 10 mm above a flat plate. The normalized amplitude (**b**–**c**) and phase (**d**–**e**) of this flow is shown for stimulus frequencies of 0.1, 1, 10 and 100 Hz for a sphere with a 3 mm radius. The *inset panels* compare the amplitude **c** and phase **e** of predicted flow (*black curve*, Eq. 20) and a linearized prediction (*dashed blue curve*, Eq. 22) at the scale of a cupula. All simulations used the mean parameter values for zebrafish larvae (Table 1)

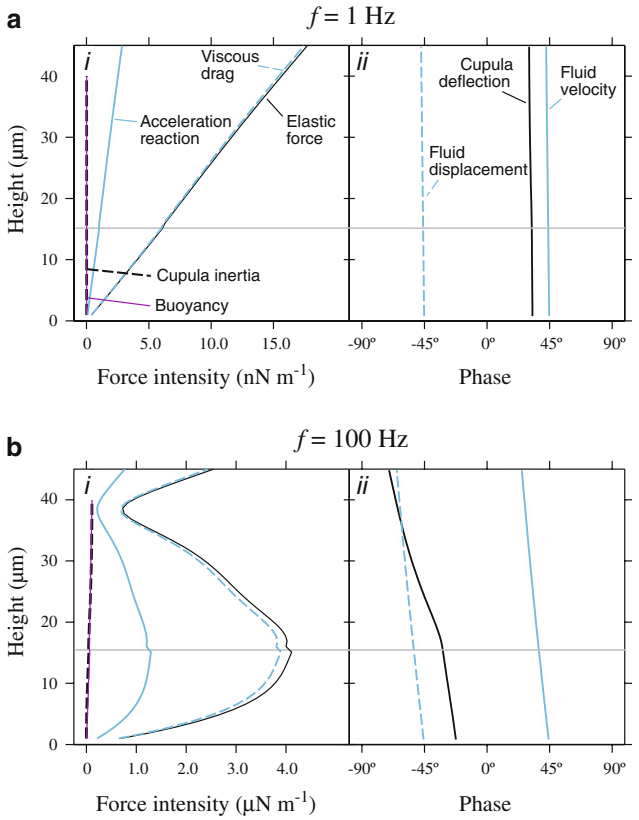

Fig. 12 Changes in the fluid–structure interaction of the cupula with frequency. (*i*) Predicted relevant force intensities (force per unit length) and (*ii*) phase of motion at stimulus frequencies of **a** $f = 1$ Hz and **b** $f = 100$ Hz predicted by the model of zebrafish larvae (Table 1). *Horizontal gray lines* denote the height of the kinocilia, where the cupula transitions in flexural stiffness

Effects of cupular morphology on filtering

Although the form of the frequency response is predicted to be similar among all superficial neuromasts, the cut-off frequency and maximum amplitude of sensitivity vary with cupular morphology. Sensitivity is especially affected by the number of hair cells and the height of their kinocilia. Our results suggest that the high stiffness of the kinocilia causes hair cells to stiffen the proximal cupula and thereby act to reduce mechanical sensitivity (Fig. 4a).

The deflections of a kinocilium are resisted by their linkage to the stereocilia of a hair cell. We have modeled this linkage as a linear torsion spring, as in biophysical models of hair cells (Howard and Hudspeth 1988), and found the frequency responses of the cupula are almost indistinguishable from that of a beam that is rigidly fixed to the epithelium (Fig. 5). Furthermore, varying the spring stiffness of the hair bundles showed little effect on cupular sensitivity unless reduced to an unrealistically small level (Fig. 4i). The stiffness of the hair bundles and the gating spring play an integral role in the biophysics of hair cells (Hudspeth and Corey 1977; Hudspeth and Jacobs 1979; Hudspeth 1989) and thereby affects the receptor potentials generated by the deflection of the hair bundle. However, our model does suggest that these deflections are independent of bundle torsion stiffness and are instead dominated by the fluid–structure interaction of the cupula.

This minor role for the torsion spring of the hair bundles of superficial neuromasts contrasts the micromechanics of canal neuromasts. In canal neuromasts, the cupula behaves as a rigid body that slides along the epithelium against the stiffness of the hair bundles (van Netten and Kroese 1987; van Netten 1988). This coupling between the cupula and the hair cells causes the neuromast to resonate like an underdamped oscillator with a peak in sensitivity at 100–1,000 Hz (van Netten 2006). Therefore, the essential role of hair bundle stiffness in the filtering by the canal neuromasts may partially be attributed to the rigid body dynamics of the cupula.

The cupular matrix is composed of a highly compliant glycosaminoglycan gel (Sato 1962) that, in some species, includes fibrils of unknown composition (Jielof et al. 1952; Münz 1979; Kelly and van Netten 1991). These fibrils likely increase the Young's modulus and hence the flexural stiffness of the cupular matrix. Our sensitivity analysis (Fig. 4vii) suggests that the cupula is most sensitive when the matrix is composed of a Young's modulus close to that of zebrafish larvae ($E = 21$ Pa; McHenry and van Netten 2007). However, greater flexural stiffness in the distal cupula enhances sensitivity (Fig. 6) by transmitting greater bending moments and hence cupular deflection at the stereocilia. Furthermore, larger cupulae may benefit from the greater structural integrity of a stiffer material. For example, the cupulae of the Mexican blind cavefish (*Astyanax fasiatus mexicanus*) are about ten times the height of zebrafish (Teyke 1990) and nearly three orders of magnitude more stiff (Peleshanko et al. 2007). This high material stiffness is likely aided by the presence of fibrils within the matrix that are not present in zebrafish larvae (Münz 1979; McHenry and van Netten 2007).

In conclusion, our model suggests that there are multiple levels of mechanical filtering between a hydrodynamic stimulus and the neurobiological response of a superficial neuromast. The cupula is predicted to respond to pressure-driven flows with bandpass filtering (Figs. 3, 4, 5, 6) that is generated by the combined effects of the boundary layer and the fluid–structure interaction of the cupula with flow near the body's surface. The cupula filters in a similar manner with a vibrating sphere stimulus, but a sphere creates a boundary layer with a two-gain frequency response. For either stimulus, the cupula is sensitive to the velocity of flow near to the body's surface (Fig. 8) and serves as a low-pass filter (Figs. 9, 10). The maximum amplitude and cut-off frequency of this response varies with the dimensions and Young's modulus of the cupular matrix and the number and height of hair cell kinocilia (Figs. 4, 5, 6). These results demonstrate that the sensitivity of a superficial neuromast depends critically on the hydrodynamics of a stimulus, the boundary layer that it generates, and the fluid and structural dynamics of the cupula.

Acknowledgments This research was supported by National Science Foundation grants to MJM (IOS-0723288 and IOB-0509740). Although no experiments were performed for this work, we have complied with the "Principles of animal care", publication no. 86-23, revised 1985 of the National Institute of Health, and also with the current laws of the USA and The Netherlands.

References

Anderson EJ, McGillis WR, Grosenbaugh MA (2001) The boundary layer of swimming fish. J Exp Biol 204:81–102

Arkett SA, Mackie GO (1988) Hair cell mechanoreception in the jellyfish *Aglantha digitale*. J Exp Biol 135:329–342

Batchelor GK (1967) An introduction to fluid dynamics. Cambridge University Press, New York

van Bergeijk WA (1967) Introductory comments on lateral line function. In: Cahn PH (ed) Lateral line detectors. Indiana University Press, Bloomington, pp 73–81

Bleckmann H (1994) Reception of hydrodynamic stimuli in aquatic and semiaquatic animals. Prog Zool 41:1–115

Bone Q, Ryan KP (1978) Cupular sense organs in *Ciona* (Tunicata: Ascidiacea). J Zool Lond 186:417–429

Budelmann BU (1989) Hydrodynamic receptor systems in invertebrates. In: Coombs S, Gorner P, Münz H (eds) The mechanosensory lateral line. Springer, Berlin, pp 607–631

Budelmann BU, Bleckmann H (1988) A lateral line analogue in cephalopods: water waves generate microphonic potentials in the epidermal head lines of *Sepia* and *Lolliguncula*. J Comp Physiol A 164:1–5

Cahn PH, Shaw E (1962) The first demonstration of lateral line cupulae in the Mugiliformes. Copeia 1962:109–114

Coombs S, Conley RA (1997) Dipole source localization by the mottled sculpin. 2. The role of lateral line excitation patterns. J Comp Physiol A 180:401–415

Coombs S, Hasting M, Finneran J (1996) Modeling and measuring lateral line excitation patterns to changing dipole source locations. J Comp Physiol A 178:359–371

Coombs S, Montgomery JC (1999) The enigmatic lateral line system. In: Fay RR, Popper AN (eds) Comparative hearing: fish and amphibians. Springer, New York

Coombs S, van Netten SM (2006) The hydrodynamics and structural mechanics of the lateral line system. In: Shadwick RE, Lauder GV (eds) Fish biomechanics. Elsevier, New York, pp 103–139

Curcic-Blake B, van Netten SM (2006) Source location encoding in the fish lateral line canal. J Exp Biol 209:1548–1559

Daniel TL (1981) Fish mucus: in situ measurements of polymer drag reduction. Biol Bull 160:376–382

Denton EJ, Gray JAB (1983) Mechanical factors in the excitation of clupeid lateral lines. Proc R Soc Lond 218:1–26

Denton EJ, Gray JAB (1982) The rigidity of fish and patterns of lateral line stimulation. Nature 297:679–681

Devarakonda R, Barth FG, Humphrey JAC (1996) Dynamics of arthropod filiform hairs. IV. Motion in air and water. Proc R Soc Lond 351:933–946

Dinklo T (2005) Mechno- and electrophysiological studies on cochlear hair cells and superficial lateral line cupulae. Doctoral dissertation, Neurobiophysics, University of Groningen

Flock A (1965) Electron microscopic and electrophysiological studies on the lateral line canal organ. Acta Otolaryngol Suppl 199:1–90

Gere JM (2001) Mechanics of materials. Nelson Thornes Ltd, Cheltenham

Harris GG, Frishkopf LS, Flock A (1970) Receptor potentials from hair cells of the lateral line. Science 167:76–79

Harris GG, Milne DC (1966) Input-output characteristics of the lateral-line organs of *Xenopus laevis*. J Acoust Soc Am 40:32–42

Hassan ES (1985) Mathematical analysis of the stimulus of the lateral line organ. Biol Cybern 52:23–36

Highham TE, Day SW, Wainwright PC (2006) Multidimensional analysis of suction feeding performance in fishes: fluid speed, acceleration, strike accuracy and the ingested volume of water. J Exp Biol 209:2713–2725

Hofer B (1908) Studien über die Hautsinnesorgane der Fische. I. Die funktion der seitenorgane bei den fischen. Ber Kgl Bayer Biol Versuchsstation München 1:115–164

Howard J, Hudspeth AJ (1988) Compliance of the hair bundle associated with gating of mechanoelectrical transduction channels in the bullfrog saccular hair cell. Neuron 1:189–199

Hudspeth AJ (1982) Extracellular current flow and the site of transduction by vertebrate hair cells. J Neurosci 2:1–10

Hudspeth AJ (1989) How the ear's works work. Nature 341:397–404

Hudspeth AJ, Corey DP (1977) Sensitivity, polarity, and conductance change in the response of vertebrate hair cells to controlled mechanical stimuli. Proc Natl Acad Sci 74:2407–2411

Hudspeth AJ, Jacobs R (1979) Stereocilia mediate transduction in vertebrate hair cells. Proc Natl Acad Sci 76:1506–1509

Humphrey JAC, Devarakonda R, Iglesias I, Barth FG (1993) Dynamics of arthropod filiform hairs. I. Mathematical modeling of the hair and air motions. Philos Trans R Soc Lond B 340:423–444

Hussey RG, Good BJ, Reynolds JM (1967) Oscillation of two cylinders in liquid helium. Phys Fluids 10:89–95

Janssen J (2004) Lateral line sensory ecology. In: Emde GVD, Mogdans J, Kapoor BG (eds) The senses of fish: adaptations for the reception of natural stimuli. Kluwer, Boston, pp 231–264

Jielof R, Spoor A, de Vries H (1952) The microphonic activity of the lateral line. J Physiol 116:137–157

Kalmijn AJ (1988) Hydrodynamic and acoustic field detection. In: Atema J, Fay RR, Popper AN, Tavolga WN (eds) Sensory biology of aquatic animals. Springer, New York, pp 83–130

Kalmijn AJ (1989) Functional evolution of lateral line and inner ear sensory systems. In: Coombs S, Gorner P, Münz H (eds) The mechanosensory lateral line. Springer, Berlin, pp 187–215

Kelly JP, van Netten SM (1991) Topology and mechanics of the cupula in the fish lateral line. Variations of cupular structure and composition in three dimensions. J Morphol 207:23–36

Kroese ABA, Schellart NAM (1987) Evidence for velocity and acceleration-sensitive units in the trunk lateral line of the trout. J Physiol 394:2212–2221

Kroese ABA, van der Zalm JM, van den Bercken J (1978) Frequency response of the lateral-line organ of *Xenopus laevis*. Pfluegers Arch 375:167–175

Kroese ABA, van der Zalm JM, van den Bercken J (1980) Extracellular receptor potentials from the lateral-line organ of *xenopus laevis*. J Exp Biol 86:63–77

Kuiper JW (1967) Frequency characteristics and functional significance of the lateral line organ. In: Cahn PH (ed) Lateral line detectors. Indiana University Press, Bloomington, pp 105–121

Lamb H (1911) On the uniform motion of a sphere through a viscous fluid. Philos Mag 21:112

Lamb H (1945) Hydrodynamics. Article 361. Dover, New York

McHenry MJ, Lauder GV (2005) The mechanical scaling of coasting in zebrafish (*Danio rerio*). J Exp Biol 208:2289–2301

McHenry MJ, van Netten SM (2007) The flexural stiffness of superficial neuromasts in the zebrafish (*Danio rerio*) lateral line. J Exp Biol 210:4244–4253

Mogdans J, Krother S, Engelmann J (2004) Neurobiology of the fish lateral line: adaptations for the detection of hydrodynamic stimuli in running water. In: Emde GVD, Mogdans J, Kapoor BG (eds) The senses of fish: adaptations for the reception of natural stimuli. Narosa Publishing House, New Delhi, pp 265–287

Montgomery J, Coombs S (1992) Physiological characterization of lateral line function in the antarctic fish *Trematomus-Bernacchii*. Brain Behav Evol 40:209–216

Moore AMF, Cobb JLS (1986) Neurophysiological studies on the detection of mechanical stimuli in *Ophiura ophiura*. J Exp Mar Biol Ecol 104:125–141

Münz H (1979) Morphology and innervation of the lateral line system in *Sarotherodon niloticus* (L.) (Cichlidae, Teleostei). Zoomorphologie 93:73–86

Münz H (1985) Single unit activity in the peripheral lateral line system of the cichlid fish *Sarotherodon niloticus* L. J Comp Physiol A 157:555–568

Münz H, Claas B, Fritzsch B (1984) Electroreceptive and mechanoreceptive units in the lateral line of the axolotl *Ambystoma-mexicanum*. J Comp Physiol A 154:33–44

van Netten SM (1988) Laser interferometric microscope for the measurement of nanometer vibrational displacements of a light-scattering microscopic object. J Acoust Soc Am 83:1667–1674

van Netten SM (2006) Hydrodynamic detection by cupulae in a lateral line canal: functional relations between physics and physiology. Biol Cyber 94:67–85

van Netten SM, Kroese ABA (1987) Laser interferometric measurements on the dynamic behavior of the cupula in the fish lateral line. Hear Res 29:55–61

Oseen, CW (1910) Über die Stokessche Formel und über eine verwandte Aufgabe in der Hydrodynamik. Ark Mat Astr Fys 6

Peleshanko S, Julian MD, Ornatska M, McConney ME, LeMieux MC, Chen N, Tucker C, Yang Y, Liu C, Humphrey JAC, Tsukruk VV (2007) Hydrogel-encapsulated microfabricated haircell mimicking fish cupulae neuromast. Adv Mater 19:2903–2909

Pozrikidis C (1997) Shear flow over a protuberance on a plane wall. J Eng Math 31:29–42

Sarpkaya T (1986) Force on a circular cylinder in viscous oscillatory flow at low Keulegan–Carpenter numbers. J Fluid Mech 165:61–71

Sato M (1962) Studies on the pit organs of fishes V. The structure and polysaccharide histochemistry of the cupula pit organ. Annot Zool Jpn 35:80–88

Scharrer E (1932) Experiments on the function of the lateral-line organs in the larvae of *Amblystoma punctatus*. J Exp Zool 61:109–114

Schlichting H (1979) Boundary-layer theory. McGraw-Hill, New York

Schulze FE (1861) Uber die Nervenendigung in den sogenannten Schleimkanälen der Fische und über entsprechende Organe der durch Kiemen athmenden Amphibien Arch Anat Pizysiol Lpz 759–769

Shatz LF (2005) Slender body method for slender prolate spheroids and hemispheroids on planes in linearized oscillatory flow. Phys Fluids 17:113603

Stokes GG (1851) On the effect if the internal friction of fluids on the motion of pendulums. Trans Camb Philos Soc 9:8–106

Stuart JT (1963) Unsteady boundary layers. In: Rosenhead L (ed) Laminar boundary layers. Clarendon Press, Oxford, pp 349–407

Teyke T (1988) Flow field, swimming velocity, and boundary layer: parameters which affect the stimulus for the lateral line organ in blind fish. J Comp Physiol A 163:53–61

Teyke T (1990) Morphological differences in neuromasts of the blind cave fish *Astyanax-Hubbsi* and the sighted river fish *Astyanax-Mexicanus*. Brain Behav Evol 35:23–30

Van Trump WJ, McHenry MJ (2008) Lateral line morphology and sensitivity in zebrafish larvae (*Danio rerio*). J Exp Biol 211:2105–2115

Wakiya S (1961) Effect of a submerged object on a slow viscous flow. Res Rep Fac Eng Niigata Univ Jpn 10:15–24

Wakiya S (1963) Effect of a plane wall on the impulsive motion of a sphere in a viscous fluid. J Phys Soc Jpn 19:1401–1408

Weast RC (1987) CRC handbook of chemistry and physics, vol 68

Wainwright SA, Biggs WD, Currey JD, Gosline JM (1976) Mechanical design in organisms. Princeton University Press, Princeton

Williams RE, Hussey RG (1972) Oscillating cylinders and the Stokes' paradox. Phys Fluids 15:2083–2088